Earth, Planets and Space
a SpringerOpen Journal

FRONTIER LETTER Open Access

Microchemical and structural evidence for space weathering in soils from asteroid Itokawa

Michelle S Thompson[1*], Roy Christoffersen[2], Thomas J Zega[1] and Lindsay P Keller[3]

Abstract

Here we report microchemical and microstructural features indicative of space weathering in a particle returned from the surface of asteroid Itokawa by the Hayabusa mission. Space weathering features include partially and completely amorphous rims, chemically and structurally heterogeneous multilayer rims, amorphous surface islands, vesiculated rim textures, and nanophase iron particles. Solar-wind irradiation is likely responsible for the amorphization as well as the associated vesiculation of grain rims. The multilayer rims contain a nanocrystalline outer layer that is underlain by an amorphous inner layer, and both have compositions that are distinct from the underlying, crystalline orthopyroxene grain. The multilayer rim features could be derived from either radiation-induced sputter deposition or vapor deposition from micrometeorite impact events. The amorphous islands on grain surfaces have a distinctive morphology and composition suggesting that they represent surface deposits of melt derived from micrometeorite impact events. These observations indicate that both irradiation damage and micrometeorite impacts play a role in surface modification and space weathering on asteroid Itokawa.

Keywords: Hayabusa; Itokawa; Space weathering; Irradiation; Micrometeorite impact; Airless body; Transmission electron microscopy; Sample return analysis

Findings

Introduction

Due to their exposure to interplanetary space, the surfaces of airless bodies are continually being modified by solar ions, predominantly from the solar wind, and through micrometeorite impacts. These modifications are collectively known as space weathering, and they cause changes in the chemistry, mineralogy, microstructure, and morphology of soils exposed on airless body surfaces. The culmination of these processes alters the optical properties of surface materials by reddening and darkening soil reflectance spectra and attenuating characteristic absorption bands (Hapke 2001; Clark et al. 2002; Chapman 2004). Understanding these spectral changes is important as they are theorized to contribute to the discrepancies between reflectance spectra acquired from meteorites and asteroids that prevent us from matching meteorite samples to their parent-body sources, e.g., ordinary chondrites and S-type asteroids (Binzel et al. 1996). Investigation of the nature of the space weathering process and quantification of its effects can provide information fundamental to understanding the evolution of airless body surfaces from remote sensing data.

Space weathering processes are occurring on the surfaces of airless bodies across the solar system, including the Moon and both near-Earth and main-belt asteroids. Until the recent return of the Hayabusa mission from S-type asteroid Itokawa (Nakamura et al. 2011), sample-based studies of space weathering focused exclusively on lunar soils returned from the Apollo missions and select asteroidal and lunar regolith breccia meteorites (Bibring et al. 1972; Hapke et al. 1975; Keller and McKay 1993, 1997; Bernatowicz et al. 1994; Pieters et al. 2000; Taylor et al. 2001; Noble et al. 2005, 2011). These investigations indicated that space weathering features form as a product of two primary processes: (i) solar wind ion irradiation, which can cause partial or complete amorphization of material and possible chemical changes in grain rims, as well as erosion, transport, and redeposition of material on grain surfaces induced by ion sputtering, and (ii) micrometeorite impact events which promote melting, vaporization, and the recondensation of the target and

* Correspondence: mst@lpl.arizona.edu
[1]Lunar and Planetary Laboratory, University of Arizona, 1629 E University Blvd, Tucson, AZ 85721, USA
Full list of author information is available at the end of the article

impactor material. Each of these processes has the potential to produce reduced iron nanoparticles ($npFe^0$), which can be formed through vapor or sputter deposition onto the rims of surface grains and also as interior particles in lunar agglutinate glass grains. This $npFe^0$ contributes to the changes in optical properties we see in space-weathered materials (Noble et al. 2007).

The Hayabusa mission successfully returned thousands of dust particles from the surface of S-type asteroid Itokawa (Nakamura et al. 2011). Mineralogical analysis of several particles revealed compositions consistent with LL5-6 chondrites (Nakamura et al. 2011). The link between these particles and LL chondrites was further confirmed by oxygen isotope analyses (Yurimoto et al. 2011; Nakashima et al. 2013). The return of these samples has provided the strongest evidence yet for the long-held idea that the ordinary chondrites, the most common meteorites in our collections, are sourced from the populous S-type asteroids. The dissimilarity, however, between the reflectance spectra of Itokawa's surface and LL-type chondrites (mainly reddening in the asteroid spectrum) suggests that space weathering processes have occurred on the surface of Itokawa (Hiroi et al. 2006).

Previous investigations of Hayabusa particles for detection of space weathering features were initially completed on ten particles, five of which exhibited characteristics consistent with space weathering processes (Noguchi et al. 2011). A further detailed analysis of 12 particles was performed, and these results have shown that several grains exhibit space weathering features including radiation-damaged rims (partially and completely amorphous), Fe nanoparticles, vesiculated textures, and chemically distinct, surface-deposited rims (Noguchi et al. 2014). Thus far, Noguchi et al. (2014) suggest that the primary mechanism for surface alteration on asteroid Itokawa is solar wind irradiation including sputtering and ion implantation. However, given the small number of particles examined, further detailed investigation is required for a comprehensive understanding of space weathering processes on Itokawa as well as other airless bodies. Here we report on previously unrecognized space weathering characteristics in a particle returned from the surface of Itokawa.

Methods

We investigated three samples (RA-QD02-0042-01, RA-QD02-0042-02, and RA-QD02-0042-03) of one particle, which was collected from Room A of the sample catcher on the Hayabusa spacecraft. These samples were prepared for analysis using ultramicrotomy by the Hayabusa mission curation team. The grain, originally measuring 96 μm in diameter, was sliced into many ultrathin (<100 nm) sections. Each sample contains multiple slices that were placed on C-coated Cu-support grids for analysis using transmission electron microscopy (TEM). The original particle was exposed to the atmosphere during its preparation for analysis in the TEM, but its total exposure time was less than 6 h (Noguchi et al. 2014). These samples, and a subset of the space weathering features they exhibited, were described in previous investigations (Noguchi et al. 2011, 2014).

We investigated the samples using several analytical scanning transmission electron microscopes (STEM instruments) including (1) a 200-keV FEI Osiris ChemiS-TEM equipped with a high brightness field-emission gun (X-FEG), quad-annular silicon drift detector (SDD) for energy-dispersive X-ray spectroscopy (EDS), and both dark-field (DF) and bright-field (BF) STEM detectors previously located at FEI headquarters (Portland, OR, USA); (2) a 200-keV JEOL 2500SE analytical S/TEM (JEOL Ltd., Tokyo, Japan) at NASA Johnson Space Center equipped with a Thermo thin-window Li-drifted Si [Si(Li)] EDS detector and BF and DF STEM detectors (Thermo Fisher Scientific, Waltham, MA, USA); and (3) a 200-keV JEOL 2010F S/TEM at Arizona State University equipped with a DF STEM detector and EDAX thin-window Si(Li) EDS system. Analysis of the assemblages within the slices included imaging via conventional TEM techniques, STEM BF and DF, and high-angle annular dark field (HAADF). Phase identification was determined using selected-area electron-diffraction (SAED) patterns and high-resolution TEM (HRTEM) imaging. All SAED patterns were measured both manually with Adobe Photoshop and with the Crystallographic Processing Software Package (CRISP) based on calibrated camera constants. Indexing of SAED patterns was based on appropriate lattice constants and verified through simulated patterns calculated with the CrystalMaker software package. Grain compositions were measured with EDS on the JEOL 2500SE and the JEOL 2010 F using spectral imaging with scanned probe sizes between 1 and 3 nm, count rates varying between 5,200 and 20,000 cps, and a dwell time of 50 μs for both instruments. EDS spectra were quantified using the Cliff-Lorimer method, with K-factors determined from in-house standards.

Results

General petrography

The particle studied here is primarily composed of an orthopyroxene grain that exhibits high strain contrast with smaller, subsidiary grains of olivine (<5 μm) and plagioclase (<15 μm) attached to the orthopyroxene. These minerals are traceable through adjacent slices in the microtome sections. There are also Fe- and Fe-Ni sulfide minerals (<1 μm in size) both embedded within the pyroxene grain and located on its periphery, in multiple adjacent slices on the grid. Individual grains of Fe-Ni metal, identified as kamacite, were also found on the exterior rim of this assemblage. The presence of each

phase was confirmed with EDS spectral imaging and SAED (Figure 1). The lath-like nature of this assemblage (shards separated by void space) is characteristic of chattering, an artifact produced during microtome sample preparation and, in this respect, is similar to samples observed from the STARDUST mission (Zolensky et al. 2006).

Space weathering features

We analyzed over 30 individual slices for microchemical and microstructural evidence of space weathering. We observed several features indicative of space weathering that occur in very close spatial proximity to one another along the outer rims of the grains that collectively comprise the particle within these slices. Nearly all the individual slices that we examined exhibit some degree of space weathering. While space weathering features occur in several different mineral types, the extent and degree of their manifestation differ significantly. We discuss the space weathering features in detail below.

Partial amorphization

There are zones in the particle rim that have characteristics consistent with partial-to-complete solid-state amorphization of the underlying crystalline grains. The width and nature of these zones vary significantly depending on the mineralogy of the underlying grain. The partially amorphous regions are not continuous over the entire rim of the particle but instead occur in localized regions that extend laterally along the rims of individual grains in this assemblage for hundreds of nanometers (Figure 2). In the low-Ca orthopyroxene grain, there is a partially amorphous zone that forms an irregular boundary with the underlying crystalline grain and extends between 10 to 60 nm into the interior (Figure 2b). Within these zones, there are localized nanocrystalline regions which range from 5 to 15 nm in size. Amorphous material locally surrounds and intermixes with the crystalline domains. EDS mapping shows that the partially amorphous rims on the orthopyroxene have compositions identical to the underlying crystalline material, indicating that their only difference from the underlying material is their lack of long-range structural order. In addition, these zones of partial amorphization contain isolated Fe nanoparticles, the details of which we describe below.

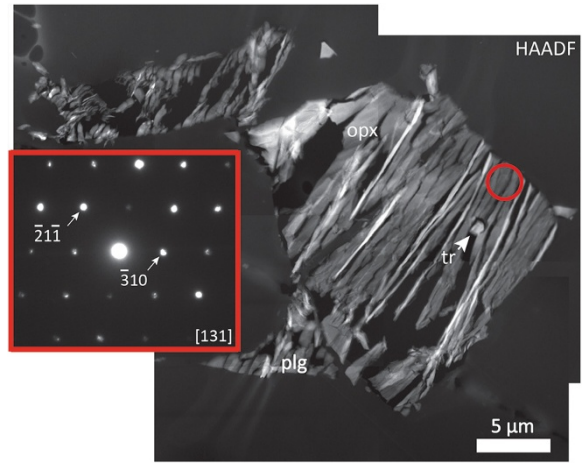

Figure 1 TEM data and EDS maps of particle RA-QD02-0042-02. HAADF image of one slice of the assemblage. The particle is primarily composed of orthopyroxene (opx) with minor plagioclase (plg), and troilite (tr). The lathic morphology is a result of chattering, a common texture observed in ultramicrotomed samples of small particles. The SAED pattern (inset) was collected from the region outlined by the red circle on the HAADF image and is indexed to orthopyroxene.

Complete amorphization

An outer rim of complete amorphization occurs on the plagioclase grain which contrasts to the zones of partial amorphization found on the orthopyroxene. This rim is also thinner than that on the orthopyroxene, extending only approximately 20 nm from the outer edge into the crystalline material, and is of more uniform thickness (Figure 2c,d). The composition of the plagioclase rim is identical to the underlying crystal.

We note that we looked for solar flare tracks in both the orthopyroxene and plagioclase grains, but none were observed.

Multilayer rims

Local regions along the outer margin of the orthopyroxene grain are comprised of altered rim material with both underlying and overlying layers, each 2 to 5 nm thick (Figure 3a,b). Laterally, the layers extend over tens to hundreds of nanometers of the grain rim. The multilayer feature is traceable through multiple adjacent slices and occurs in the same region of the grain rim in each slice. EDS spectral imaging shows that the outer and inner layers have compositions that differ from one another and from the underlying grain interior (Figure 3). Quantified compositional profiles were extracted from EDS spectral images along a line through the rims and into the grain interior (*cf.* Figure 3c,d,e,f,g). The outermost layer in the multilayer rim displays an approximately 7 at% depletion in Si relative to the bulk crystal interior and approximately 4 at% enrichments in both Fe and Mg. In contrast, the inner layer has an approximately 10 at% enrichment in Si, an approximately 3 at% depletion in Fe, and an approximately 10 at% depletion in Mg relative to the grain interior. The estimated errors are <1.7 at% (1σ) without an absorption correction.

The multilayer rim exhibits microstructural heterogeneity that correlates with the chemical differences. The

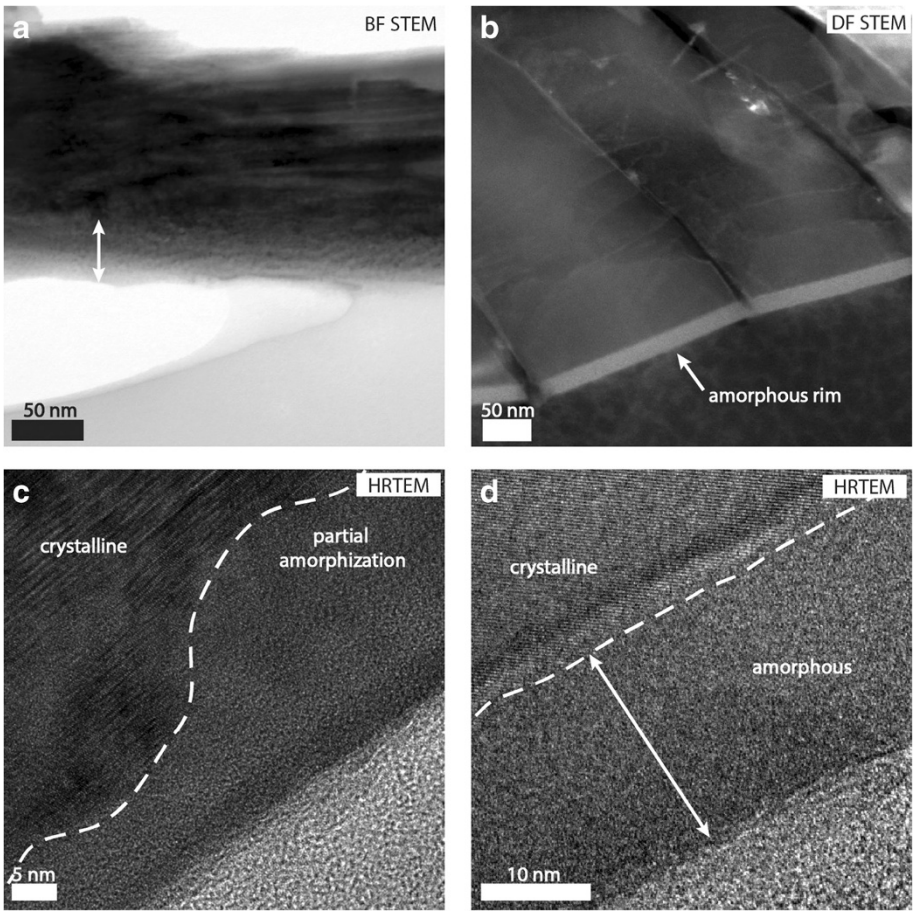

Figure 2 TEM data on the orthopyroxene and plagioclase grains. (a) BF STEM image of a region of the rim of orthopyroxene with arrow indicating the zone of partial amorphization. **(b)** DF STEM image of the amorphous rim on the plagioclase grain, indicated by the arrow. **(c)** HRTEM image of the highly variable depth and degree of amorphization within the orthopyroxene. **(d)** HRTEM image of the rim of complete amorphization showing uniform the thickness on the plagioclase.

outer, Si-depleted, Fe- and Mg-enriched layer is composed of nanocrystalline domains, as shown in the HRTEM image in Figure 3h. Fourier transform diffractograms of several HRTEM images of this nanocrystalline region give reflections with *d*-spacings of 0.223 nm, which is close (within error) to several orthopyroxene spacings, e.g., (122); olivine spacings, e.g., (140) or (122); Fe metal spacings, e.g., (101); or MgO spacings, e.g., (111) or (200). HRTEM images show that the underlying Si-enriched layer is completely amorphous and abruptly transitions into the crystalline grain interior.

Amorphous islands

In localized areas of the grain rim, there are isolated regions of material that protrude tens of nanometers from the grain surface. These island-like regions are superimposed on top of the Si-enriched layer of the multilayer rims, suggesting that they were deposited on top of the grain edge. The chemical composition of these islands is different from the underlying bulk crystal (Figure 4b,c,d,e). The islands contain significant S (approximately 4 at%) that is not present in the grain interior. In addition, EDS spectral imaging reveals that the islands are enriched in Fe and Mg and depleted in Si relative to the underlying bulk crystal (Figure 4b,c,d,e). HRTEM images of these islands show that they are completely amorphous.

Vesiculated textures

There are both well- and poorly developed vesicles in the partially amorphous rim of the orthopyroxene grain (Figure 4f,g). These vesicles occur 10 to 30 nm below the grain rim surface and vary in size between 5 and 20 nm. The well-developed vesicles are emplaced in a partially amorphous matrix and cause bulging of the grain rim around them. These features are not the product of sample preparation or beam damage, having been identified in pyroxene, a relatively beam-stable mineral in the TEM, in both ultramicrotomed and focused-ion beam sections. These vesicles are present in very low concentrations, occurring in localized regions of only a few slices.

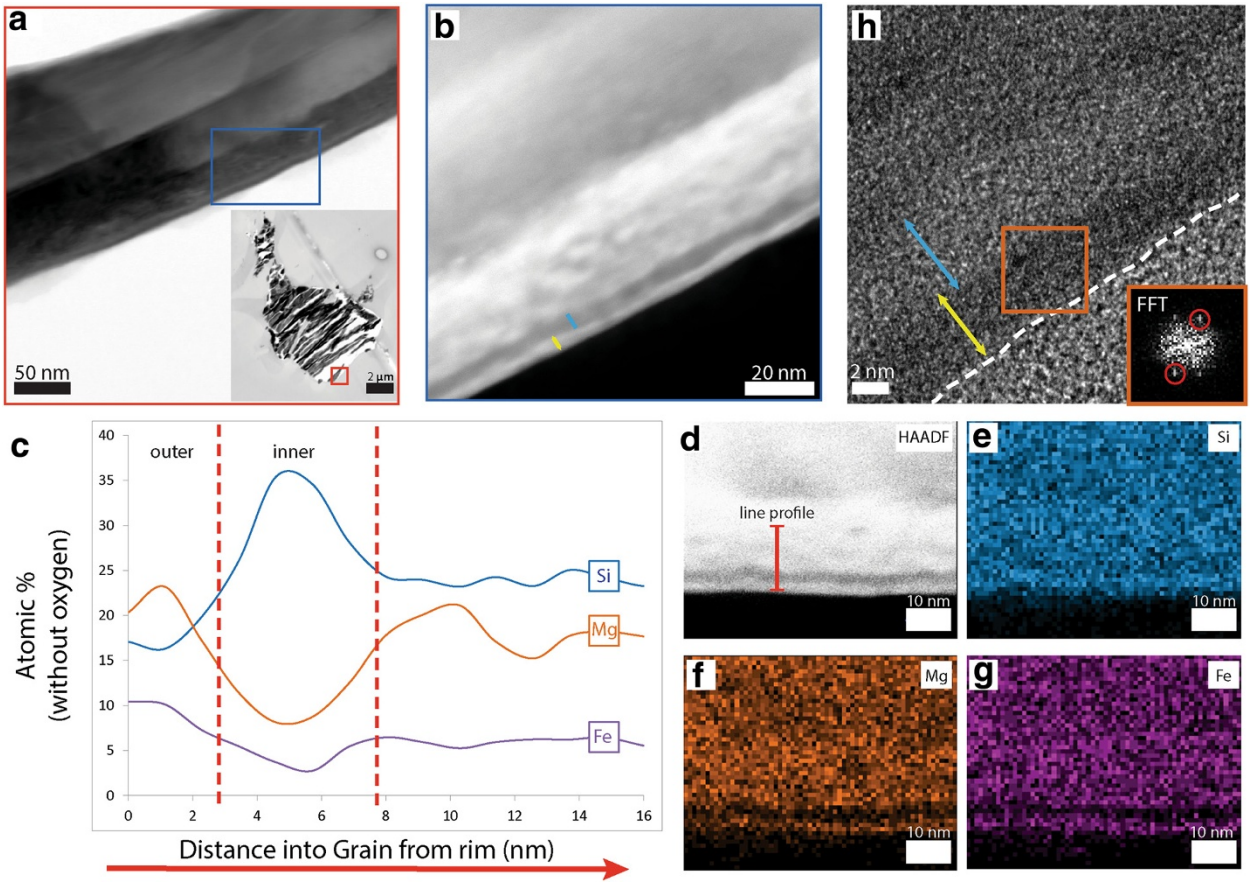

Figure 3 TEM and EDS data of the multilayer rims on orthopyroxene. (a) BF image of the multilayer rim on the edge of the pyroxene grain. **(b)** HAADF image of the rim with outer and inner layers indicated by arrows. **(c)** Line profile acquired from the edge of the grain, through the multilayer rim to the interior. Red dashed lines indicate boundaries between layers on the grain exterior and the underlying grain interior. **(d)** HAADF image of the multilayer rim and location of the line profile. **(e-g)** EDS spectral images of the multilayer rim. **(h)** HRTEM image of the multilayer rim with yellow arrows indicating the zone of nanocrystallinity and blue arrows indicating amorphous region. The white dashed line indicates the edge of the grain, and the inset FFT shows discrete reflections measuring 0.223 nm, indicating nanocrystalline nature of the outermost layer.

Nanophase iron particles

In three of the individual slices analyzed, Fe nanoparticles were identified in high-resolution EDS spectral mapping in regions of the orthopyroxene rim, but were not identified in any other mineral type sections. These findings indicate that the overall abundance of Fe nanoparticles in the analyzed sample as a whole is low (e.g., Figure 5). Where they occur, the nanophase Fe grains are uniformly distributed in their confined regions, occurring up to 60 nm from the exterior grain rim, and are emplaced in a partially amorphous matrix. The individual particles are uniform in size, each measuring between 2 and 3 nm. EDS mapping on an area containing a particularly high concentration of nanophase Fe particles indicates that the grains are composed primarily of Fe, with no associated Mg or S signatures (Figure 5b,c,d,e,f). These nanoparticles may be Fe oxide or metallic Fe, though the relative depletion in O (Figure 5f) in the profile of the grain may suggest metallic Fe.

Discussion

The variety of individual space weathering features we observed in these samples indicates that these grains have experienced a complex processing history on the surface of Itokawa. The nature of the observed features suggests that they developed with contributions from both ion radiation processing, almost certainly associated with solar wind ions, and micrometeorite impact events. Below we discuss the specific implications of each of the observed features for surface processing on Itokawa.

Amorphization features

The amorphous zones (both partial and complete, which have identical compositions to the underlying grain) are

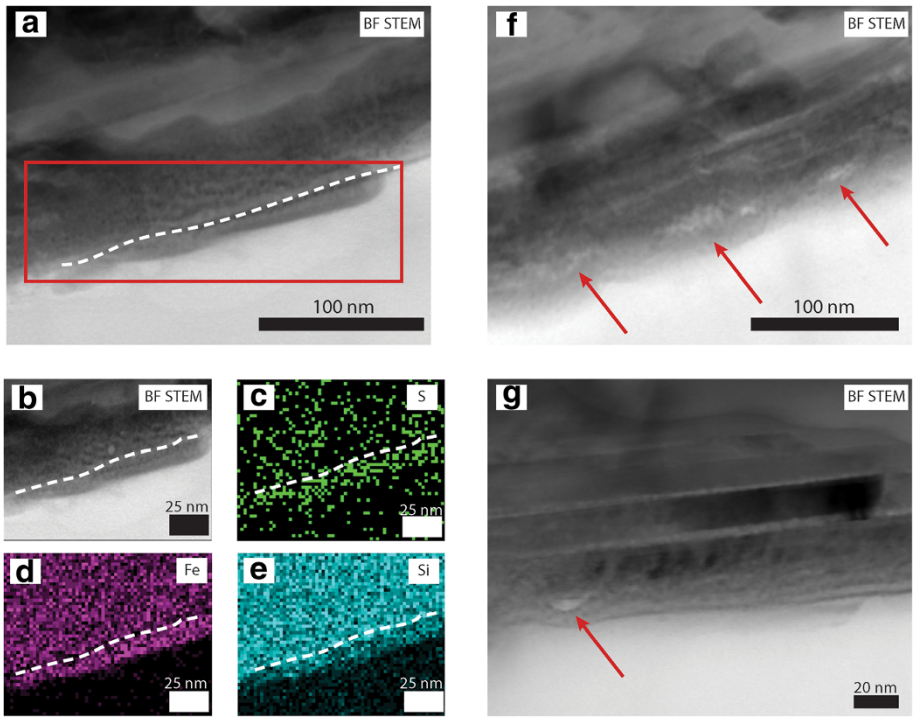

Figure 4 TEM and EDS data of other space weathering features in these grains. (a) BF STEM image of the amorphous island deposited on the grain rim. The white dashed line indicates the original grain surface. **(b-e)** BF STEM and EDS spectral images of the island feature showing enrichments in Fe and S relative to the underlying grain, as located by the red box in **(a)**. **(f)** BF STEM image of poorly developed vesicles, as indicated by arrows in the partially amorphous matrix of the orthopyroxene rim. **(g)** BF STEM image of a well-developed vesicle, indicated by red arrow in the partially amorphous orthopyroxene rim.

attributed to solar wind ion irradiation effects. Solar ions, mostly 1 to 4 keV H^+ and He^+, have been estimated by Noguchi et al. (2014) using the Stopping and Range of Ions in Matter (SRIM) Monte Carlo atomic collisions code (Ziegler et al. 2008) to penetrate between 27 and 51 nm (H and He, respectively) into the grain interior from the rim. These simulations were performed for forsteritic (Fo_{70}) olivine (Noguchi et al. 2014). The simulations and the observed thickness of the orthopyroxene rims on our samples (thickness <60 nm) are also consistent with the width of ion-amorphized layers in experimental samples, the width of rims on lunar regolith grains, and previously described Itokawa samples (Keller and McKay 1997; Carrez et al. 2002; Loeffler et al. 2009; Noguchi et al. 2011, 2014). In comparison, the plagioclase grain rim exhibits a more consistent degree of damage (i.e., complete amorphization) and is uniformly more narrow (<25 nm) than the average width of the orthopyroxene rim.

Plagioclase is, however, more susceptible to electron beam damage that may have artificially widened the rim or altered its chemistry and microstructure. In order to account for this sensitivity, we imaged the rim for structure before completing any prolonged analytical work that would have otherwise damaged the sample before we had a chance to assess long-range order. This experimental approach ensured that the thickness and amorphous nature of the grain rim was indigenous to the samples and not an artifact of TEM analysis. After completing spectral imaging, we did observe the effects of beam damage on the plagioclase as the interface between the rim and underlying crystalline material retreated further into the grain interior, revealing that the amorphous layer had increased in thickness.

The discrepancy between the nature and thickness of the orthopyroxene and plagioclase rims suggests three possibilities. (1) The grains had relatively similar solar wind exposure times, and the different characteristics of the rims primarily reflect variations in the solid-state response of the two phases to solar wind ion irradiation. Most notably, this could include differences in the critical ion fluence needed to amorphize the two phases. (2) The solid-state response of both phases to irradiation is relatively similar, and the grains were simply exposed directly to solar wind ions for different lengths of time. Finally, (3) both factors contributed to the development of these features.

We are currently not aware of any direct, quantitative experimental comparison of the ion processing behavior or relative amorphization fluences of orthopyroxene

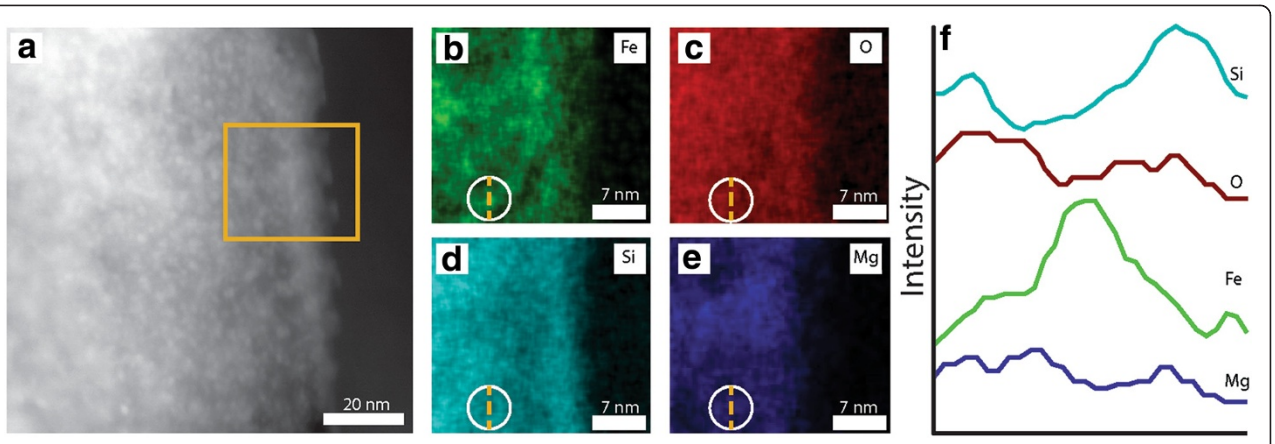

Figure 5 TEM and EDS data of nanophase Fe in the rim of orthopyroxene. (a) HAADF image of the orthopyroxene grain rim showing a high concentration of Fe nanoparticles. **(b-e)** EDS maps of the region indicated by the yellow box in **(a)**. An individual particle is indicated by a white circle in **(b-e)**. **(f)** Intensity profiles for Si, O, Fe, and Mg taken across the identified particle, indicated by a dashed yellow line. Note the obvious Fe peak, the relatively consistent Mg and O concentrations, and the Si enrichment bordering the particle.

compared to plagioclase under conditions applicable to the solar wind. The ion processing behavior of pyroxene relative to a wide range of other silicates has, however, been investigated under irradiation similar to the regime expected for the solar wind (Wang and Ewing 1992; Wang et al. 1998a,b; Christoffersen and Keller 2011). These studies suggest that structures in which the Si-O tetrahedral sites are more polymerized, as in plagioclase, with a greater variety of interstitial sites, are generally much more susceptible to radiation-induced amorphization (Wang and Ewing 1992). This prediction is consistent with the well-known greater susceptibility of feldspars to electron-beam damage relative to pyroxene. As such, the differences in the degree of partial or complete amorphization between the plagioclase and orthopyroxene may reflect this difference.

With regard to the differences in width between the feldspar and pyroxene grain rims, irrespective of their degree of structural amorphization, several factors may play a role. The intrinsic penetration range of ions into the two minerals is determined by differences in the nuclear-elastic and electronic stopping power of their collective constituent atoms and by the structure's atomic density (Ziegler et al. 2008). Based on SRIM calculations, the maximum in deposited collision energy by H^+ and He^+ at solar wind energies occurs at respective depths of approximately 11 and 23 nm for plagioclase and 8 and 20 nm for orthopyroxene. This maximum is likely to correspond to the rim width, because the deposited energy falls off rapidly beyond the maximum. Based on these relations, rims in feldspar can be expected to be wider than those in pyroxene, all other factors being equal. These simulations assume ion bombardment at fixed energies with one ion type, unlike the energy range and multi-ion composition of the solar wind, and only account for normal incidence of irradiation. Nonetheless, these are important first-order estimates for understanding the development of irradiated rims on airless body materials.

As noted above, there is the possibility that differences in exposure time may also play a role that is superposed on differences in the ion processing behavior of the two minerals. The narrow width of the rim on the plagioclase grain analyzed here (<25 nm) is significantly less than those observed on plagioclase grains in mature lunar soils, which range from 10 to 100 nm in thickness, with an average thickness of approximately 50 nm (Zhang and Keller 2012). The smaller rim thickness on the plagioclase grain from Itokawa would seem to suggest that its exposure time is therefore less than that for a mature lunar soil. However, although the orthopyroxene and plagioclase grains are part of one coherent assemblage now, it is possible that they did not exist cohesively during their entire surface exposure lifetime. The observed spatial relationship could be a product of sample collection methods or the amalgamation of grains during a recent surface event, e.g., an impact. Such an event could group together grains with vastly different exposure times resulting in variable radiation damage features.

The lack of distinct solar flare tracks may speak to the exposure history of this individual particle which our microtome slices are sourced from. It is possible that the lack of tracks identified here is a result of the inherent difficulty in identifying solar flare tracks in pyroxene minerals that exhibit a high concentration of strain features, including this grain. Another possibility, however, is that these grains were exposed for a very short period of time on the surface of Itokawa, preventing the accumulation of tracks in high enough density to measure. However, we note the difficulty in constraining relevant

surface residence times of material on Itokawa from the analysis of one single particle.

Multilayer rim features

The chemically heterogeneous layers we report here are distinct from the composite redeposition rims previously reported (Noguchi et al. 2011, 2014). The rims previously described are comprised of an outermost totally amorphous region, whereas the rims we report on here contain a multilayer, mixed nanocrystalline, and amorphous morphology. We hypothesize two possible formation mechanisms for these features, or a combination of these processes, described below. The significantly different composition of the multilayer rims relative to the underlying grain (Figure 3) suggests that the rims could be the product of vapor deposition from a micrometeorite impact of an adjacent grain with a different chemical composition. However, similar features in lunar soils attributed to micrometeorite impact events are typically amorphous because the vapor-deposited material is quenched at low temperatures, preventing the development of crystalline domains. As a result, the nanocrystalline nature of the outer layer in the multilayer rims may argue against this formation mechanism as it suggests that there was sufficient time for at least small grains to crystallize. A nearby heating event, e.g., a subsequent micrometeorite impact in the local surface region, could have provided enough thermal energy to slow quenching and allow for the outer layer to recrystallize.

Alternative processes for forming the chemically heterogeneous multilayer rims could also involve preferential solar ion sputtering of the grain surface itself, sputter deposition of material derived from surrounding grains, or a combination of the two processes (Hapke 2001). For silicate minerals, the compositional relations that can develop in the outer rims of grains involved in either of these processes, especially involving relative changes in the constituent cation concentrations like those observed here in the orthopyroxene rims, are still not well understood. Therefore, it remains possible that either of these sputtering processes, or a sequence of the two processes, may have contributed to forming the compositional relationships in the inner and outer layers in the orthopyroxene rims.

Amorphous islands

The amorphous islands are similar to lunar glass features that have been attributed to micrometeorite impact events (Keller and McKay 1997). Their relief from the underlying grain, completely amorphous crystal structure, and different chemistry when compared to the bulk grain beneath are similar to impact glasses in lunar soils that are 'splashed' onto the surface from adjacent material. We therefore infer that micrometeorite impacts produced the amorphous islands that we observe in these Itokawa samples.

Fe nanoparticles

$NpFe^0$ particles have been produced experimentally through both irradiation experiments and simulated micrometeorite impacts using laser irradiation (Sasaki et al. 2001). Previous studies have attributed individual formation mechanisms to nanoparticles with specific chemistries. $NpFe^0$ particles associated with Mg and S are attributed to micrometeorite impact events and subsequent vapor deposition (Noguchi et al. 2011). These particles often occur close to the surface of the grain, in a matrix of completely amorphous material. In contrast, particles emplaced deeper into the grain that are not associated with Mg or S but are instead purely Fe are suggested to have formed through radiation processing events (Noguchi et al. 2011). The data on the Fe nanoparticles observed in our Hayabusa particles suggest that they were produced through ion irradiation events because they occur in a matrix that is isochemical with the underlying grain and are also located deeper in the grain in a matrix of partially amorphous material. The relatively low concentration of these particles when compared to lunar samples may suggest a short exposure time on the surface of Itokawa, preventing the accumulation of high volumes of Fe nanoparticles. If this low concentration were characteristic of the population of space-weathered grains on Itokawa as a whole, it may indicate that the spectral reddening characteristic of S-type asteroids can be produced with only a small amount of $npFe^0$.

Vesiculated textures

The vesiculated textures observed in our assemblages have been reproduced in experimental samples subjected to irradiation (Hishmeh et al. 1994). Such high concentrations of vesicles are rare in grain rims from mature lunar soils (Keller and McKay 1997), although vesiculated grain rims are commonplace in friable lunar breccias (Noble et al. 2005). Noble et al. (2005) proposed that the vesiculated rims result from thermal processing of the solar wind implanted grains. A similar thermal event may have produced the vesiculated rims we observe on the Itokawa grains.

The space weathering features observed in samples from Itokawa suggest that while radiation from solar energetic ions does play a significant role in surface alteration of this body, observed impact glasses suggest that micrometeorite impacts also contribute to its significant and complex processing history. The surface environments of the Moon and Itokawa are different, e.g., potentially higher resurfacing rates on Itokawa resulting in

shorter grain exposure times and lower surface gravity resulting in lower retention of impact products. However, the data presented here suggest that the *processes* altering their surface characteristics are similar, although the *features* these processes generate are variable.

Conclusions

We examined the detailed microstructure and chemistry of particle RA-QD02-0042 returned by the Hayabusa mission. The particle contains an assemblage with a diverse mineralogy including orthopyroxene, plagioclase, olivine, Fe and Fe-Ni sulfides, and Fe-Ni metal. The data suggest that the grains on the surface of Itokawa have a complex processing history with contributions from both micrometeorite impacts and radiation processing events. Several characteristics, including the differences we observe in concentration and distribution of $npFe^0$ particles in these samples, vary from previous observations of lunar soils. The discrepancies in these features are likely a product of different surface modification environments between the Moon and Itokawa and indicate that we should revisit our lunar soil collection for analysis in a new context.

Abbreviations

BF: bright field; DF: dark field; EDS: energy-dispersive X-ray spectroscopy; HAADF: high-angle annular dark field; HRTEM: high-resolution transmission electron microscopy; $npFe^0$: nanophase iron particles; TEM: transmission electron microscopy/microscope.

Competing interests

The authors declare that they have no competing interests.

Authors' contributions

Each of the authors contributed to the data collection and interpretation. The manuscript was prepared by MST with helpful contributions from co-authors. All authors read and approved the final manuscript.

Acknowledgements

We thank JAXA for the allocation of Hayabusa samples for this study. We gratefully acknowledge the use of facilities within the Leroy Eyring Center for Solid State Science at Arizona State University. We acknowledge the use of facilities and assistance from Huikai Cheng at FEI. The TEM work at the Johnson Space Center was supported in part by a grant to LPK from the NASA Laboratory Analysis of Returned Samples (LARS) program. Funding for MS Thompson is provided by the Natural Sciences and Engineering Research Council of Canada (NSERC). This research was supported in part by NASA. Three anonymous reviewers are acknowledged for their constructive comments.

Author details

[1]Lunar and Planetary Laboratory, University of Arizona, 1629 E University Blvd, Tucson, AZ 85721, USA. [2]Jacobs, NASA Johnson Space Center, Mail Code KR, Houston, TX 77058, USA. [3]NASA JSC Mail Code KR, Houston, TX 77058, USA.

Received: 7 March 2014 Accepted: 30 July 2014
Published: 13 August 2014

References

Bernatowicz TJ, Nichols RH, Hohenberg CM, Maurette M (1994) Vapor deposits in the lunar regolith. Science 264(5166):1779–1780. doi:10.1126/science.264.5166.1779-a

Bibring JP, Duraud JP, Durrieu L, Jouret C, Maurette M, Meunier R (1972) Ultrathin amorphous coatings on lunar dust grains. Science 175(4023):753–755, 10.1126/science.175.4023.753

Binzel RP, Bus SJ, Burbine TH, Sunshine JM (1996) Spectral properties of near-Earth asteroids: evidence for sources of ordinary chondrite meteorites. Science 373:946–948

Carrez P, Demyk K, Cordier P, Gengembre L, Grimblot J, D'Hendecourt L, Jones AP, Leroux H (2002) Low-energy helium ion irradiation-induced amorphization and chemical changes in olivine: insights for silicate dust evolution in the interstellar medium. Meteorit Planet Sci 37(11):1599–1614

Chapman CR (2004) Space weathering of asteroid surfaces. Ann Rev Earth Planet Sci 32:539–567

Christoffersen R, Keller LP (2011) Space radiation processing of sulfides and silicates in primitive solar systems materials: comparative insights from in situ TEM ion irradiation experiments. Meteorit Planet Sci 46(7):950–969, 10.1111/j.1945-5100.2011.01203.x

Clark BE, Hapke B, Pieters C, Britt D (2002) Asteroid space weathering and regolith evolution. In: Bottke W, Cellino A, Paolicchi P, Binzel RP (eds) Asteroids III. University of Arizona Press, Tucson, Arizona

Hapke B (2001) Space weathering from Mercury to the asteroid belt. J Geophys Res Planet 106(E5):10039–10073, 10.1029/2000JE001338

Hapke B, Cassidy W, Wells E (1975) Effects of vapor-phase deposition processes on the optical, chemical, and magnetic properties of the lunar regolith. Moon 13(1–3):339–353

Hiroi T, Abe M, Kitazato K, Abe S, Clark BE, Sasaki S, Ishiguro M, Barnouin-Jha OS (2006) Developing space weathering on the asteroid 25143 Itokawa. Nature 443(7107):56–58

Hishmeh G, Cartz L, Desage F, Templier C, Desoyer J, Birtcher R (1994) Rare gas bubbles in muscovite mica implanted with xenon and krypton. J Mater Res 9 (12):3095–3107

Keller LP, McKay DS (1993) Discovery of vapor deposits in the lunar regolith. Science 261(5126):1305–1307, 10.1126/science.261.5126.1305

Keller LP, McKay DS (1997) The nature and origin of rims on lunar soil grains. Geochim Cosmochim Acta 61(11):2331–2341

Loeffler M, Dukes C, Baragiola R (2009) Irradiation of olivine by 4 keV He^+: simulation of space weathering by the solar wind. J Geophys Res Planet 114: E03003

Nakamura T, Noguchi T, Tanaka M, Zolensky ME, Kimura M, Tsuchiyama A, Nakato A, Ogami T, Ishida H, Uesugi M, Yada T, Shirai K, Fujimura A, Okazaki R, Sandford SA, Ishibashi Y, Abe M, Okada T, Ueno M, Mukai T, Yoshikawa M, Kawaguchi J (2011) Itokawa dust particles: a direct link between S-type asteroids and ordinary chondrites. Science 333(6046):1113–1116, 10.1126/science.1207758

Nakashima D, Kita NT, Ushikubo T, Noguchi T, Nakamura T, Valley JW (2013) Oxygen three-isotope ratios of silicate particles returned from asteroid Itokawa by the Hayabusa spacecraft: a strong link with equilibrated LL chondrites. Earth Planet Sci Lett 379:127–136

Noble SK, Keller LP, Pieters CM (2005) Evidence of space weathering in regolith breccias I: lunar regolith breccias. Meteorit Planet Sci 40(3):397–408

Noble SK, Pieters CM, Keller LP (2007) An experimental approach to understanding the optical effects of space weathering. Icarus 192(2):629–642

Noble SK, Keller LP, Pieters CM (2011) Evidence of space weathering in regolith breccias II: asteroidal regolith breccias. Meteorit Planet Sci 45(12):2007–2015

Noguchi T, Nakamura T, Kimura M, Zolensky ME, Tanaka M, Hashimoto T, Konno M, Nakato A, Ogami T, Fujimura A, Abe M, Yada T, Mukai T, Ueno M, Okada T, Shirai K, Ishibashi Y, Okazaki R (2011) Incipient space weathering observed on the surface of Itokawa dust particles. Science 333(6046):1121–1125, 10.1126/science.1207794

Noguchi T, Kimura M, Hashimoto T, Konno M, Nakamura T, Zolensky ME, Okazaki R, Tanaka M, Tsuchiyama A, Nakato A, Ogami T, Ishida H, Sagae R, Tsujimoto S, Matsumoto T, Matsuno J, Fujimura A, Abe M, Yada T, Mukai T, Ueno M, Okada T, Shirai K, Ishibashi Y (2014) Space weathered rims found on the surfaces of the Itokawa dust particles. Meteorit Planet Sci 49(2):188–214, 10.1111/maps.12111

Pieters CM, Taylor LA, Noble SK, Keller LP, Hapke B, Morris RV, Allen CC, McKay DS, Wentworth S (2000) Space weathering on airless bodies: resolving a mystery with lunar samples. Meteorit Planet Sci 35(5):1101–1107, 10.1111/j.1945-5100.2000.tb01496.x

Sasaki S, Nakamura K, Hamabe Y, Kurahashi E, Hiroi T (2001) Production of iron nanoparticles by laser irradiation in a simulation of lunar-like space weathering. Nature 410(6828):555–557

Taylor LA, Pieters CM, Keller LP, Morris RV, McKay DS (2001) Lunar mare soils: space weathering and the major effects of surface-correlated nanophase Fe. J Geophys Res Planet 106:27985–27999

Wang LM, Ewing RC (1992) Ion-beam-induced amorphization of complex ceramic materials—minerals. MRS Bull 17(05):38–44

Wang SX, Wang LM, Ewing RC, Doremus RH (1998a) Ion beam-induced amorphization in $MgO–Al_2O_3–SiO_2$. I. Experimental and theoretical basis. J Non-Cryst Solids 238(3):198–213

Wang SX, Wang LM, Ewing RC, Doremus RH (1998b) Ion beam-induced amorphization in $MgO–Al_2O_3–SiO_2$. II. Empirical model. J Non-Cryst Solids 238(3):214–224

Yurimoto H, K-i A, Abe M, Ebihara M, Fujimura A, Hashiguchi M, Hashizume K, Ireland TR, Itoh S, Katayama J (2011) Oxygen isotopic compositions of asteroidal materials returned from Itokawa by the Hayabusa mission. Science 333(6046):1116–1119

Zhang S, Keller LP (2012) Rates of space weathering in lunar regolith grains. In: Abstracts of the Meteoritical Society Meeting. Cairns, Australia

Ziegler JF, Biersack JP, Ziegler MD (2008) SRIM, the Stopping and Range of Ions in Matter. Lulu Press, Raleigh

Zolensky ME, Zega TJ, Yano H, Wirick S, Westphal AJ, Weisberg MK, Weber I, Warren JL, Velbel MA, Tsuchiyama A, Tsou P, Toppani A, Toka N, Tomeoka K, Teslich N, Taheri M, Susini J, Stroud R, Stephan T, Stadermann FJ, Snead CJ, Simon SB, Simionovici A, See TH, Robert F, Rietmeijer FJM, Rao W, Perronnet MC, Papanastassiou DA, Okudaira K (2006) Mineralogy and petrology of comet 81P/wild 2 nucleus samples. Science 314(5806):1735–1739, 10.1126/science.1135842

doi:10.1186/1880-5981-66-89
Cite this article as: Thompson *et al.*: **Microchemical and structural evidence for space weathering in soils from asteroid Itokawa.** *Earth, Planets and Space* 2014 **66**:89.